
Article:
Bird, S.M., Galloway, J.M., Rawlings, A.E. et al. (2 more authors) (2015) Taking a hard line with biotemplating: cobalt-doped magnetite magnetic nanoparticle arrays. Nanoscale, 7 (16). 7340 - 7351.

https://doi.org/10.1039/c5nr00651a

Journal Name

RSCPublishing

ARTICLE

Cite this: DOI: 10.1039/x0xx00000x

Taking a Hard Line with Biotemplating: Cobalt-Doped Magnetite Magnetic Nanoparticle Arrays

Scott M. Bird,[a] Johanna M. Galloway,[b] Andrea E. Rawlings,[a] Jonathan P. Bramble,[a] and Sarah S. Staniland[a]

Received 00th January 2015,
Accepted 00th January 2015

DOI: 10.1039/x0xx00000x

www.rsc.org/

Rapid advancements made in technology, and the drive towards miniaturisation, means that we require reliable, sustainable and cost effective methods of manufacturing a wide range of nanomaterials. In this bioinspired study, we take advantage of millions of years of evolution, and adapt a biomineralisation protein for surface patterning of biotemplated magnetic nanoparticles (MNPs). We employ soft-lithographic micro-contact printing to pattern a recombinant version of the biomineralisation protein Mms6 (derived from the magnetotactic bacterium Magnetospirillum magneticum AMB-1). The Mms6 attaches to gold surfaces via a cysteine residue introduced into the N-terminal region. The surface bound protein biotemplates highly uniform MNPs of magnetite onto patterned surfaces during an aqueous mineralisation reaction (with a mean diameter of 90±15 nm). The simple addition of 6% cobalt to the mineralisation reaction maintains the uniformity in grain size (with a mean diameter of 84±14 nm), and results in the production of MNPs with a much higher coercivity (increased from ≈156 Oe to ≈377 Oe). Biotemplating magnetic nanoparticles on patterned surfaces could form a novel, environmentally friendly route for the production of bit-patterned media, potentially the next generation of ultra-high density magnetic data storage devices. This is a simple method to fine-tune the magnetic hardness of the surface biotemplated MNPs, and could easily be adapted to biotemplate a wide range of different nanomaterials on surfaces to create a range of biologically templated devices.

1. Introduction

The development of nanomaterials is a major driving force behind the advancement of technology. Nanoscale materials exhibit novel physical and chemical properties due to at least one dimension being on the nanoscale (i.e. 1-100 nm), a size range between bulk macroscopic materials and individual atoms. Magnetic nanoparticles (MNPs) are no exception, having been the subject of extensive studies across a wide range of fields.[1-3] MNPs can be found in an ever-increasing number of commercial applications, including catalysis,[4] environmental contaminant removal,[5] in magnetic fluids,[6] as contrast agents for magnetic resonance imaging,[7] and targeted drug delivery.[8] MNPs, when patterned and immobilised onto surfaces, are well suited for use in data storage applications, with the potential to extend the storage capacity of magnetic hard disk drives to meet an ever-expanding demand.[9]

Within traditional magnetic storage devices, data is written onto a granular ferromagnetic film (e.g. Co alloys).[10] Bits of information are written by magnetically orientating the grains, to be read as binary code. Since IBM introduced the first commercial magnetic hard disk in 1956 storage densities have increased more than 20 million-times, with today's devices having capacities in excess of 500 Gbit in^{-2}.[10] Although there are a number of alternative data storage technologies on the market today, in terms of cost per Gb, magnetic data storage remains significantly cheaper.[10] While the demand for higher density data storage is expected to continue to grow current devices are approaching their physical limits, as reducing the grain size of the granular recording media leads to enhanced thermal demagnetisation effects and the onset of superparamagnetism.[11]

Bit-patterned media is a new generation of magnetic data storage that increases storage densities by utilising arrays of nanoscale magnetic islands.[9, 10, 12] Each bit of information is written to a magnetic island, potentially forming devices with storage capacities in the Tbit in^{-2} range.[10] However, there are many challenges to overcome before bit-patterned media is realised for ultra-high density data storage, including

developing a reliable and cost effective method to uniformly pattern nanoscale magnetic islands precisely.[10]

Biology offers an attractive and green approach for controlling the bottom-up manufacturing of materials. Biomineralisation is ubiquitous in nature, occurring in almost all groups of organisms, from bacteria to humans, via the application of biomineralising proteins. Proteins have evolved with the capability of controlling the formation of complex organic-mineral structures under mild aqueous conditions, and there are over 60 natural biominerals.[13] Several biomineralising proteins and peptides have been identified or modified to facilitate the formation of a wide range of different materials in vitro.[14] Work has also focused on utilising biomolecules to biomineralise inorganic materials that are not found in nature including: gold,[15] silver,[16] FePt,[17] and CoPt.[18, 19] For example, the cage protein ferritin has been used to template the growth of MNPs.[20, 21, 22] Although these MNPs have been subsequently attached to surfaces, recording experiments have so far shown that this system is only suitable for low-density recording (12.6 Gbit in^{-2}).[23]

Magnetotactic bacteria are remarkable organisms, capable of biomineralising magnetite (Fe_3O_4) MNPs inside specialised lipid organelles called magnetosomes.[24-26] Arakaki et al.[27] identified the biomineralisation protein Mms6 from the magnetosome of the bacterium Magnetospirillum magneticum AMB-1. Mms6 is thought to have a hydrophobic membrane embedded N-terminus, and an acidic C-terminal region located in the magnetosome interior. The C-terminal has been shown to strongly bind iron, and is believed to initiate the nucleation of magnetite in vivo.[27, 28] Arakaki et al.[27] then in collaboration with our group,[29 30] and others,[31] have shown that Mms6 is able to control the formation of consistent MNPs of magnetite in vitro under mild reaction conditions, and Mms6 on a surface binds iron oxide MNPs from aqueous solution.[32]

Through the combination of top-down and bottom-up methods, our group recently published a new, integrated and adaptive approach for the production of microscale patterns of magnetite MNPs.[33, 34] This was achieved by micro-contact printing (μCP) a protein resistant polyethylene glycol (PEG) self-assembled monolayer (SAM) pattern onto gold. The remaining areas were backfilled with a SAM containing carboxylic acid residues. This formed a patterned functionalised surface to selectively promote or resist the attachment of Mms6. Mms6 binds to the carboxylic acid moieties via its N-terminal amine when activated by an Ethyl-(dimethylaminopropyl) carbodiimide (EDC) and N-hydroxysuccinimide (NHS).[35] The Mms6 patterned surface was then subject to a mineralisation reaction to form patterns of uniform MNPs of magnetite under mild, aqueous reaction conditions. The Mms6 protein is dual purpose; controlling the size and shape of the nanoparticles, and anchoring these particles to the surface.

Here we report a new method of immobilising Mms6 on a patterned surface, by using Mms6 protein (which contains no native cysteine residues) engineered to contain an N-terminal cysteine (cys-Mms6). In previous work,[33, 34] achieving consistency in the patterning and orientation of Mms6 was challenging because the EDC/NHS attachment is not specific for the N-terminal amine group, but could also target accessible lysine residues. The sulfur in the N-terminal cysteine of cys-Mms6 allows the protein to self-assemble onto the gold surface via a thiol-gold bond. This speeds up and simplifies the protein patterning as it removes the additional steps of the attachment SAM and activation via EDC and NHS. Cys-Mms6 is more likely to be correctly orientated for biomineralisation, offering a simplified approach to creating an active, efficient Mms6 biotemplating patterned surface.

Also, magnetite is a magnetically soft material (i.e. has a low coercivity). This is unsuitable for use in data storage, as a high coercivity is required to retain recorded data on hard disks. We have shown previously that, when in a bulk solution, Mms6 is able to template the formation of cobalt-doped magnetite, which has a higher coercivity than magnetite.[30] Here, we have mineralised cobalt-doped magnetite MNPs on a patterned surface biotemplated by cys-Mms6. Controlled doping of cobalt allows the magnetic properties of the biomineralised MNP arrays to be tuned. In this study, for the first time we combine our innovative and simplified gold-cysteine attachment of cys-Mms6, with the synthesis of 6% cobalt-doped magnetite MNP arrays. This study demonstrates the adaptability of this simple method, introducing a new bioinspired approach that could be used for the production of a wide range of biotemplated nanomaterials on surfaces. More specifically, we present a significant step towards making a new, greener method for developing bit-patterned media.

2. Experimental

Synthesis of MNP Arrays

Synthesis of recombinant cysteine-tagged Mms6 (cys-Mms6): The plasmid pBPTNHTCmms6 was constructed using a conventional restriction enzyme cloning strategy. The sequence encoding the mature form of Mms6 from Magnetospirillum magneticum AMB-1 was ligated into a pTTQ18 derived vector. This vector encodes an octa-histidine (His8) tag sequence upstream of the mms6 gene. The vector was then modified by site-directed mutagenesis to introduce a single cysteine residue between the tag and the mms6 gene (see Supplementary Methods), and successful mutants were confirmed by DNA sequencing. pBPTNHTCmms6 was transformed into E. coli strain BL21 (DE3) RP (Stratagene) and was cultured in Super Broth autoinduction media (Formedium),[36] including carbenicillin (100 μg mL^{-1}) and chloramphenicol (34 μg mL^{-1}) antibiotics, for >24 hours at 37˚C, with constant shaking at 225 rpm. Following this, cells were harvested by centrifugation and resuspended in phosphate buffered saline (PBS; 137 mM NaCl, 3 mM KCl, 10 mM Na_2HPO_4 and 1.5 mM KH_2PO_4 at pH 7.4) to produce a 20% (w/v pellet/buffer) solution before being lysed by sonication. The lysate was cleared by centrifugation, and the pellet

resuspended in 6 M Guanidine hydrochloride (GuHCl) and 50 mM Tris at pH 8 and incubated at room temperature for 1 hour to denature the Mms6 inclusion bodies. Further centrifugation was then used to remove any insoluble material before the supernatant was mixed with 1 mL Nickel-NTA resin (Expedeon) for 1 hour at 4°C to bind the Mms6 fusion protein via the His8 tag. The resin was then transferred to a gravity flow column and washed in a solution of 50 mM Tris, 6 M GuHCl and 30 mM imidazole at pH 8. The fusion protein was eluted in 50 mM Tris, 6 M GuHCl and 300 mM imidazole, also at pH 8. Following this, the protein was rapidly diluted into a solution of 500 mM NaCl and 50 mM Tris at pH 8 to refold the cysteine-tagged Mms6 protein and was concentrated using an Amicon centrifugal concentrator (Merck Millipore) to reduce the volume. Finally, the protein was dialyzed against 500 mM NaCl to remove the Tris and stored at -80˚C. The presence and purity of the His8 tagged Mms6 was confirmed by Coomassie stained SDS-PAGE and western blot (Supplementary Figure 1S) with detection via a horseradish peroxidase conjugated 5xHis monoclonal antibody (Qiagen).

Preparation of gold surfaces: Gold surfaces were evaporated onto clean glass microscope slides. The slides were cleaned via 5 minute sonication in: 1% Decon 90, Milli-Q water, methanol, and Milli-Q water. The slides were dried in a nitrogen stream, immersed in a piranha solution (H_2SO_4 70%: H_2O_2 30% v/v) for 10 minutes, rinsed with Milli-Q water and dried in nitrogen. 5 nm of chromium was evaporated onto the clean sides to form an adhesion layer, followed by 50 nm of gold in an Edwards Auto 360 thermal evaporator. These slides were then scribed and broken to form ≈1 cm^2 substrates for patterning.

Preparation of polymer stamps for micro-contact printing (*μCP*): Stamps were formed by mixing Sylgard 184 poly(dimethylsiloxane) (PDMS) (Dow Corning) in a 10:1 (w/w) ratio of prepolymer to curing agent. This mixture was stirred thoroughly, and then vacuum desiccated until all the trapped air bubbles were removed. Silicon masters with microscale line patterns were cleaned in ethanol, and then dried in a nitrogen stream. The mixture was then poured over the silicon masters and vacuum desiccated for a second time. Flexible polymer stamps for μCP were cut from the masters after curing at 60°C for >24 hours, and were soaked in ethanol for >16 hours before use to remove any uncured polymer before use.

μCP of protein resistant SAMs: Poly-ethylene glycol (PEG) terminated thiols have been shown to be resistant to protein binding,[37] and were used in previous work to resist the attachment of Mms6 to gold surfaces.[33, 34] In this work, an anti-biofouling surface was formed by μCP PEG SAMs onto gold surfaces (cleaned in a piranha solution for 5 minutes, rinsed in Milli-Q water, dried in a nitrogen stream, rinsed in ethanol and dried in nitrogen). The PEG thiol (11-mercaptoundecyl tetra(ethylene glycol), $HS(CH_2)_{11}(OCH_2CH_2)_4OH$) (Sigma-Aldrich) was dissolved in ethanol to form a 5 mM solution. This solution was used to ink the PDMS stamps. After a 4 minute incubation, the excess ink was pipetted from the surface, and the stamps were dried in a nitrogen stream. The inked and dried PDMS stamp was then placed in conformal contact with a gold surface, left in place for 4 minutes, then removed. This only formed an ordered PEG SAM where the stamp was in contact with the gold surface, leaving areas of clean gold not contacted by the stamp suitable for backfilling.

Attachment of cys-Mms6: The PEG patterned substrates were immediately placed into a PBS solution at pH 7.4 containing the cys-Mms6 protein (10 μg mL^{-1}) for 1 hour. This allows the cysteine-tagged protein to bind to areas of the gold surface not covered by PEG molecules, thus selectively functionalising these areas for biomineralisation.

Mineralisation of magnetite: The protein patterned substrates were then subjected to a partial oxidation of ferrous hydroxide with potassium hydroxide (POFHK)[38] reaction, designed to form MNPs of magnetite on biotemplating surfaces.[33, 34] The patterned substrates were rinsed in Milli-Q water, and then transferred to a glass vessel containing 24.75 mL of anaerobic Milli-Q water (vacuum degassed for 1 hour and sparged with nitrogen for 1 hour to remove oxygen prior to use). The vessel was then sealed, and the water was continuously sparged with nitrogen. Reactants were dissolved into anaerobic Milli-Q water to form 0.5 M $FeSO_4 \cdot 7H_2O$, 1 M KOH and 0.5 M KNO_3 stock solutions. 2.5 mL of the $FeSO_4$ solution was then added to the reaction vessel, followed by 2.75 mL of the KOH solution. 20 mL of the KNO_3 solution was then added drop-wise over ≈5 minutes. The vessel was heated to 80°C under constant nitrogen sparging. Over this maturation period, magnetite MNPs form in both the reaction solution and onto the patterned immobilised Mms6. After 4 hours, the samples were removed, rinsed in anaerobic Milli-Q water and dried in a nitrogen stream. The excess magnetite particles that formed in the solution were collected magnetically, washed in anaerobic Milli-Q water 5 times and sealed in glass vials.

Mineralisation of 6% cobalt-doped magnetite: MNPs of 6% cobalt-doped magnetite were biotemplated onto surfaces by simply repeating the POFHK reaction (as above) with the addition of 6% cobalt. $FeSO_4 \cdot 7H_2O$ and $CoSO_4 \cdot 7H_2O$ were dissolved in anaerobic water to form 0.5 M stock solutions. 2.35 mL of the $FeSO_4$ solution followed by 0.15 mL of the $CoSO_4$ solution were added in place of the 2.5 mL of $FeSO_4$ used previously. The remainder of the mineralisation was then carried out as described above.

Characterisation

Quartz crystal microbalance with dissipation (QCM-D): The attachment of cys-Mms6 to clean and PEG coated gold surfaces was monitored with a Q-Sense E4 QCM-D (Q-Sense AB, Gothenburg, Sweden). The experiments were performed using gold coated QCM-D crystals cleaned via 5 minute sonication in Milli-Q Water, 0.4% sodium dodecyl sulfate (SDS) detergent, Milli-Q water again, dried in a nitrogen steam, UV/ozone treated for 20 minutes, followed by immersion in ethanol for 40 minutes to reduce the gold, and finally dried in a nitrogen stream. The crystals were then either transferred to an ethanol solution containing 1 mM of dissolved PEG for >16

hours and rinsed with ethanol and dried with N_2, or the clean gold crystals were used immediately.

Experiments were performed at 22˚C, with a flow rate of 50 µL min^{-1}. Degassed Milli-Q water was flowed in to the system, and the changes in frequency (Δf) and dissipation (ΔD) were recorded for the 3rd, 5th, 7th, 9th, 11th and 13th overtones. When the recorded values stabilised a 10 µg mL^{-1} solution of cys-Mms6 in PBS was flowed into the system for 1 hour, after which the flow was returned to Milli-Q water again until the recorded values stabilised. Modelling was performed following the methods used by Krzemiński et al.[39] using Qtools 2 Qsense software operating under the assumptions of the Kelvin Voigt model,[40] a hydrodynamic protein layer density of 1200 kg m^{-3} ,[41] a buffer viscosity of 0.001 kg m^{-3}, and a buffer density of 1000 kg m^{-3}.

Scanning electron microscopy (SEM): The biomineralised gold surfaces were mounted on aluminium stubs with double sided carbon tape and earthed with silver paint. SEM images were taken with a Hitachi SU8230 SEM at an accelerating voltage of 15 keV, a working distance of approximately 15 mm and processed with Zeiss SmartSEM software.

Transmission electron microscopy (TEM): The excess MNPs formed in the POFHK reactions were collected magnetically, washed, dispersed in anaerobic Milli-Q water and this solution was pipetted onto TEM grids. The grids were allowed to dry in air, before micrographs were recorded with a FEI Tecnai G2 Spirit TEM operating at 80 keV and processed with Gatan DigitalMicrograph software.

Grain size analysis: Sizing of the MNPs biotemplated onto gold by Mms6 was performed using SEM images, and sizing of the MNPs formed in solution during the POFHK reactions was performed using TEM images. The grain size of the imaged particles was recorded along the longest axes of the projection of ≈100 MNPs per sample using Image J software.[42] These data were fitted in GraphPad Prism software with a Gaussian distribution.[43]

Inductively coupled plasma emission spectrometry (ICP-ES): Gold surfaces that were completely covered in cys-Mms6 (with no patterning and no PEG) were immersed in a POFHK reaction (to form both magnetite and 6% cobalt-doped magnetite). This ensured a greater coverage of Mms6, and hence the formation an extensive layer of surface biotemplated MNPs, maximising the ICP-ES signal. The unpatterned mineralised surfaces were washed in anaerobic Milli-Q water, dried in a nitrogen stream and placed into 2 mL of aqua regia (HCl 50%: HNO_3 50% v/v). This was then sonicated for 30 minutes to dissolve the biotemplated MNPs and the gold film. The remaining glass surface was then removed, and 3 mL of Milli-Q water was added to the solution.

Excess MNPs formed in the bulk mineralisation reactions were collected magnetically, washed in anaerobic Milli-Q water and dried under vacuum. These particles were placed into a 2 mL solution of aqua regia, and completely dissolved by sonication for 30 minutes after which 3 mL of Mill-Q water was added. The MNP solutions were then analysed with ICP-ES, along with a blank reference solution of 2 mL of aqua regia and 3 mL of Milli-Q water that did not contain any dissolved nanoparticles.

To quantify the iron and cobalt content of the MNPs, ICP-ES was performed on these solutions using a Spectro Ciros Vision ICP-ES. Iron and cobalt were measured at the 238.204 nm and 228.616 nm emission lines respectively, following calibration with suitable standards.

X-ray diffraction (XRD): Unpatterned mineralised magnetite and 6% cobalt-doped magnetite surfaces were prepared in exactly the same way as for ICP-ES, but were not dissolved in aqua regia. A Siemens D5000 diffractometer was used to obtain XRD spectra of the doped and undoped surfaces in reflection mode. X-rays were generated at 40 kV and 40 mA using a Cu Kα source (average λ = 1.54178 Å). The X-rays were directed onto the surfaces mounted on non-elastic Apiezon Q Sealing Compound putty in glancing angle geometry. X-ray intensities were collected between 2θ = 15° and 70° with a position sensitive detector (in 0.025° steps and 2.5 seconds per step).

The MNPs that formed in the bulk solutions during the POFHK reactions (used to form the magnetite or cobalt-doped magnetite surfaces) were collected magnetically, washed in anaerobic Milli-Q water and dried under vacuum. These bulk control MNPs were mixed with Elmer's glue onto an acetate disk and loaded into a STOE STADI P diffractometer. X-rays were generated at 40 keV and 35 mA using a Cu Kα1 source and X-ray intensities were collected between 2θ = 15° and 70° (in 0.03˚ steps and 2.5 seconds per step). Data were analysed with DIFFRAC Plus software and compared to d-spacings from crystallographic databases.

The grain size of the MNPs was calculated from the XRD data through the application Debye-Scherrer equation.[44] This analysis was performed on the 311 peak for each sample, and a shape constant of 0.89 was used.

Vibrating sample magnetometry (VSM): Unpatterned and biomineralised surfaces were also used for magnetic characterisation. VSM was carried out on these surfaces using an Oxford Instruments Maglab VSM. The biomineralised surfaces were mounted into the VSM and the magnetic response of the samples was recorded over a field range of -10 to 10 kOe at 295 K perpendicular to the sample surface.

Magnetic force microscopy (MFM): Atomic force microscopy (AFM) topographical images were recorded on a Multimode Nanoscope III AFM operating in tapping mode with magnetised Cr/Co coated MESP tips (Bruker). The magnetic perturbations of the sample were then measured using a magnetised tip by retracing the topography at a lift height of 50 nm, and recording the phase shift of the cantilever's resonant frequency. This phase shift is proportional to the strength of magnetic attraction (negative phase shift) or repulsion (positive phase shift) between the particles and the magnetised MFM tip. These data was processed with WSxM software,[45] and the 3D images were rendered in "R" using the rgl package.[c]

3. Results and Discussion

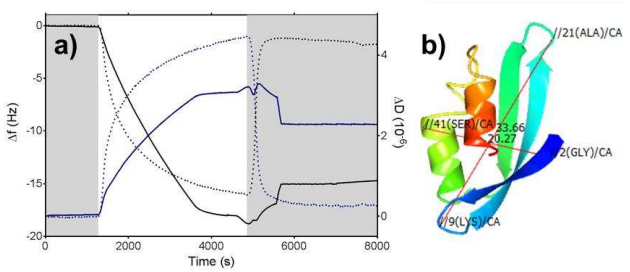

Figure 1: a) Frequency (Δf, black lines) and dissipation (ΔD, blue lines) changes of the 7th overtone recorded with QCM-D during adsorption of cys-Mms6 onto clean (solid lines) and PEG coated (dotted lines) gold quartz crystals. The grey regions indicate when ultrapure water flowed over the crystals, and the white region when a PBS buffer containing cys-Mms6 at a concentration of 10 µg mL^{-1} was applied (flow rate of 50 µL min^{-1}). b) Cartoon representation of cys-Mms6 predicted from its amino acid structure using the QUARK server,[46] and generated in CCP4mg.[47] The protein model is coloured blue at the N-terminal to red at the C-terminal, with an estimated length and width (red lines) between key amino acids displayed in Å.

Table 1. Mass coverage and visoelastic properties of cys-Mms6 adsorbed onto the clean and PEG coated gold QCM-D crystals.

Sauerbrey Values	Clean Gold Crystal	PEG Coated Gold Crystal
Mass (ng cm^{-2})	258	30
Coverage (pmol cm^{-2})	23	3
Complete Monolayer (pmol cm^{-2})	≈24	≈24
Coverage (%)	≈96	≈13
Voigt Values		
Viscosity (kg m^{-1} s^{-1})	0.0015	-
Shear (MPa)	2.2	-
Thickness (nm)	2.8	-

All modelling was performed using Qtools 2 Qsense software operating under the assumptions of the Kelvin Voigt model.[43] Sauerbrey values were calculated from the 7th overtone, and Voigt values were calculated using all the recorded overtones (3rd, 5th, 7th, 9th, 11th, 13th).

The binding of the cys-Mms6 protein to clean and PEG coated gold quartz crystals was monitored with QCM-D, and the adsorption profile of the 7th overtone is displayed in Figure 1. When exposed to a 10 µg mL^{-1} solution of cys-Mms6, it can clearly be seen that there was a significantly larger change in the recorded frequency (Δf) for the clean gold crystal than the protein resistant PEG coated gold crystal, corresponding to a greater adsorbed mass onto the clean gold surface. The Sauerbrey equation[48] was used to calculate the mass adsorbed onto the crystals, and the Voigt model[40] was applied to describe the viscoelastic properties of the adsorbed layer of the cys-Mms6 protein (Table 1).

To estimate the surface coverage of the adsorbed protein layer on the gold crystals a molecular weight of 11 kDa was assumed. This includes a 25% mass increase to account for the average water content of hydrated proteins.[49] From a model of the cys-Mms6 protein built on the Quark server[46] (folded protein length and width estimated to be 33.66 Å and 20.27 Å), we estimate a complete monolayer of the protein corresponds to approximately 24 pmol cm^{-2}. These values are summarised in Table 1, with this analysis finding that approximately 96% of the clean gold quartz crystals were covered by a layer of cys-Mms6. Only 13% coverage was seen on the PEG protected gold crystals. This suggests that almost a complete layer of cys-Mms6 adsorbs onto gold surfaces, with very limited adsorption on to a PEG coated gold surface.

A schematic illustration of the process used to synthesise biotemplated MNP patterns on surfaces, along with SEM images of the formed MNP arrays are shown in Figure 2. These SEM images show that a single high density layer of nanoparticles are formed on the protein patterned areas, with negligible mineralisation on the PEG background. This specificity of mineralisation was the case for both reaction schemes used (for magnetite and 6% cobalt-doped magnetite MNPs). Only a low density layer of small (<40nm) nanoparticles, with some collections of larger particles, formed on a bare gold surface, and there was only limited mineralisation on a gold surface completely covered with a PEG SAM (Supplementary Figure 2S). Thus, immobilised Mms6 facilitates the mineralisation of both types of MNP onto patterned surfaces, which is supported by previous work.[33, 34] Based upon the striking specificity (biomineralised nanoparticles or protein resistant PEG SAM) we observe in the SEM analysis (Figure 2), we conclude that this modified approach (the cys-Mms6 sulfur binding directly to gold) did not adversely affect the functionality of the immobilised Mms6 protein, and may have enhanced its biotemplating action.

Magnetite (Fe_3O_4) has an inverse spinel structure with ferrous (Fe^{2+}) and ferric (Fe^{3+}) ions randomly arranged at the octahedral sites, and tetrahedral sites occupied by ferrous iron.[50] This isotropic crystal structure has no preferred axis of magnetisation, resulting in magnetite being a soft magnetic material, prone to switching its magnetic orientation. However, anisotropic substitution of Co^{2+} for Fe^{2+} at the octahedral sites to produce cobalt ferrite ($CoFe_2O_4$) results in a preferred axis of magnetisation being introduced, producing a harder magnetic material, but with a greatly reduced saturation magnetisation.[51] The controlled doping of cobalt into magnetite, biotemplated by Mms6, provides a method to fine tune the coercivity and saturation magnetisation between that of magnetite and cobalt ferrite.[52] In previous work, the addition of 6% cobalt provided the largest increase in coercivity, whilst minimising the reduction in the saturation magnetisation incurred due to the addition of cobalt.[30] Therefore, the optimum value of 6% cobalt-doping into magnetite was also selected for this current study.

Here, we compare magnetite and 6% cobalt-doped magnetite MNPs, biotemplated by Mms6 onto patterned gold (hereon in referred to as $Fe_{surface}$ and $6\%Co_{surface}$ respectively), and MNPs that form in the bulk solution during these reactions (hereon in referred to as Fe_{Bulk} and $6\%Co_{Bulk}$). Further comparisons can also be drawn between the previous studies on Mms6 mediated cobalt-doped MNPs in solution,[30] as well as Mms6 mediated magnetite MNPs on surfaces via the EDC/NHS attachment method,[33, 34] ($Fe_{surface}$EN) along with Mms6 mediated 6% cobalt-doped magnetite MNPs on surfaces prepared for this study as a comparison ($6\%Co_{surface}$EN)

(Supplementary Figure 3S). The most prominent difference is clearly seen when comparing the quality of the patterns between the two methods (6%$Co_{surface}$ (Figure 2) and 6%$Co_{surface}$EN (Supplementary Figure 3S)) which show the new simpler cys-attachment methods results in cleaner, sharper, high-precision patterning.

Table 2. MNP composition determined by ICP-ES.

Sample	Fe (ppm)	Co (ppm)	% of Co
Blank	0.16±0.01	<0.01	0
Fe_{Bulk}	922±19.8	<0.01	0
6%Co_{Bulk}	905±18.1	57±1.1	5.9±0.1
$Fe_{Surface}$	231±4.6	<0.01	0
6%$Co_{Surface}$	216±4.3	13±0.3	5.7±0.1

MNPs were dissolved into a solution of aqua regia and water. A blank solution of Aqua regia and water (without any dissolved MNPs) was also analysed to confirm that Fe and Co was not present (see methods).

The presence of iron and cobalt in the MNPs formed during the POFHK reactions was confirmed with inductively coupled plasma emission spectrometry (ICP-ES) (Table 2). We considered that it might be possible that Mms6 only selects for iron ions in the 6% cobalt-doped system. This would have resulted in undoped magnetite being biotemplated onto the gold surfaces. However, cobalt was detected in an approximate 6% ratio in both the bulk solution (5.9±0.1%) and surface biotemplated (5.7±0.1%) nanoparticles. This suggests that Mms6 is able to biotemplate cobalt-doped magnetite particles onto the gold surfaces, and that there is no significant bias for iron or cobalt enrichment by the biomineralising protein. These data also show that no cobalt was detected in the magnetite only system, as expected.

Further elemental analysis was performed on the Mms6 biotemplated MNP surfaces using energy dispersive X-ray analysis (EDX), indicating the presence of the components of magnetite (iron and oxygen) on the protein patterned regions. Cobalt could not be detected in the 6%$Co_{surface}$ sample due to the Co L_α peak (776 eV) significantly overlapping with the dominant Fe L_α (705 eV) peak, coupled with the small amount of cobalt present (Supplementary Figure 4S and 5S).

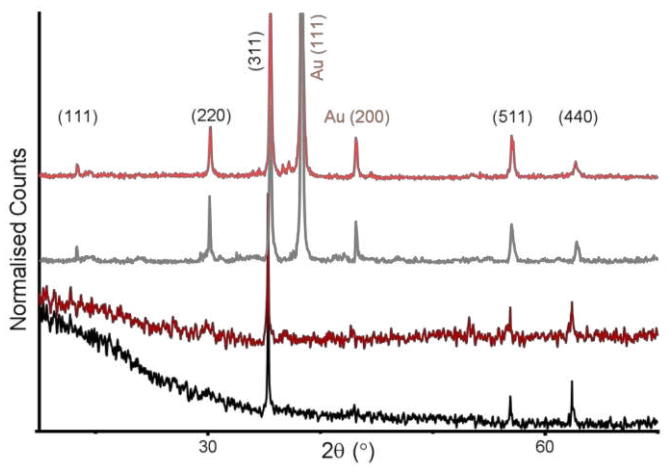

Figure 3: XRD spectra of the MNP arrays biotemplated by Mms6 and the MNPs which formed in the bulk solution during the POFHK reactions, Fe_{Bulk} (black), 6%Co_{Bulk} (dark red), $Fe_{Surface}$ (grey), 6%$Co_{Surface}$ (light red). Each spectrum is offset for clarity and peak positions for magnetite (black) and gold (gold) are labelled.

Table 3. Peak positions for maghemite, magnetite and cobalt ferrite and peak positions from the MNP samples shown in Figure 3 (all measured in Å).

Peak	Maghemite	Magnetite	Cobalt Ferrite
(111)	4.822	4.850	4.847
(220)	2.953	2.966	2.968
(311)	2.518	2.530	2.531
(511)	1.607	1.614	1.615
(440)	1.476	1.483	1.483

Peak	Fe_{Bulk}	6%Co_{Bulk}	$Fe_{Surface}$	6%$Co_{Surface}$
(111)	-	-	4.835	4.835
(220)	-	-	2.964	2.954
(311)	2.527	2.527	2.525	2.525
(511)	1.616	1.616	1.616	1.616
(440)	1.480	1.482	1.480	1.482

Based on spectra from DIFFRAC Plus software.

Crystallographic analysis was performed on all of the MNP samples using X-ray diffraction (XRD) (Figure 3), and the position of the peaks were converted to d spacings (Table 3). The MNP samples were compared to maghemite, magnetite and cobalt ferrite, which have similar crystal structures so produce similar X-ray diffraction patterns. Peaks at 2θ = 38.35° and 43.15° ($Fe_{Surface}$ and 6%$Co_{Surface}$ samples) correspond to the Au (111) and (200) reflections from the gold film on the substrate, which correlates with an XRD spectrum of a gold substrate without any PEG or cys-Mms6 attachment or subsequent MNP mineralisation (Supplementary Figure 6S).

These XRD data strongly support that the crystal structure of the surface biotemplated samples, and the control samples, are all a good match for magnetite or cobalt-doped magnetite, rather than maghemite or other iron mineral species. The relative intensities of the peaks are as expected (for example the (311) peak is the most intense). It was not possible to clearly detect the (200) or (111) peaks in the non-biotemplated bulk controls, highlighting the strong crystallinity of both the $Fe_{Surface}$ and 6%$Co_{Surface}$ biotemplated MNPs when compared to the non-biotemplated control samples.

These crystallographic data also indicate that the controls and the surface biotemplated MNPs are very stable against alteration by oxygen in the air, as there is no indication of maghemite or other oxidation products in these spectra. X-ray magnetic circular dichroism (XMCD) analysis of the comparable $Fe_{surface}$EN and 6%$Co_{surface}$EN samples (Supplementary Figure 7S) shows the $Fe_{surface}$EN MNPs biomineralised by Mms6 on the surface are of similar composition to previously reported stoichiometric magnetite,[53] while the 6%$Co_{surface}$EN samples shows a clear reduction in the Fe^{2+} octahedral peak (Supplementary Figure 7Sd) showing that cobalt is substituted into this site.[53]

Table 4. Grain size Analysis of the MNPs

Sample	Mean Size (nm)	Standard Deviation (nm)	Calculated from XRD (nm)
Fe_{Bulk}	69	36	91
$6\%Co_{Bulk}$	61	53	84
$Fe_{Surface}$	90	15	83
$6\%Co_{Surface}$	84	14	66

The size of ≈ 100 MNPs was measured per sample along the longest axis of the MNP projections in TEM and SEM images using ImageJ,[42] and were fitted using GraphPad Prism.[43]

Grain size analysis (Figure 4 and Table 4) shows that the MNPs biotemplated onto the surface are significantly larger ($Fe_{Surface}$: ≈90±15 nm and $6\%Co_{Surface}$: ≈84±14 nm) than those from the bulk solution (Fe_{Bulk}: ≈69±36 nm and $6\%Co_{Bulk}$: ≈61±53 nm). The surface biotemplated samples also appear to be highly uniform, with a much narrower size distribution ($Fe_{Surface}$ ≈15 nm and $6\%Co_{Surface}$ ≈14 nm) than those formed in the bulk solution (Fe_{Bulk} ≈ 36 nm and $6\%Co_{Bulk}$ ≈ 53 nm). These values are compared in Table 4 to the grain size of the particles calculated from the XRD data. This analysis also shows that cobalt-doping results in a reduction in particle size, but as XRD spectra was obtained with different spectrometers for the bulk and surface samples these data sets cannot be directly compared. The data suggests that the nanoparticles which form in the bulk solutions (Fe_{Bulk} ≈ 91 nm and $6\%Co_{Bulk}$ ≈ 84 nm) are larger than the surface biotemplated particles ($Fe_{Surface}$: ≈83 nm and $6\%Co_{Surface}$: ≈66 nm). However, this poor agreement could be a result of the different scan times of the spectrometers used, the noisier Fe_{Bulk} and $6\%Co_{Bulk}$ spectrums, as well as the broad particle size distributions of these samples. Overall, these data suggest that Mms6 not only initiates and controls magnetite nanoparticle growth on the surfaces and locates the MNPs formed in a pattern, but also has a strong effect on increasing the size and narrowing the size distribution of the MNPs biotemplated onto the surface.

The surface bound Mms6 biotemplates the majority of particles in the 70-100 nm diameter range. This significantly reduces the number of MNPs with a diameter <50 nm, when compared to the particles that formed in the bulk solutions. In vitro studies have shown that Mms6 aggregates into water soluble micelles in solution, which is an important feature of its iron binding capability.[31] Immobilising enzymes often results in altered activity or selectivity.[54] Likewise, it is possible that immobilising Mms6 also alters its activity, potentially by changing its ability to oligomerise; reducing a 3-dimensional assembly in bulk solution to a 2-dimensional surface (Supplementary Figure 8S). The exact nature of the changes to the protein when it is immobilised onto a surface is yet to be determined, but the surface could stabilise the proteins biotemplating action. Also, the surface bound protein is only able to bind to the underside of the nucleating and growing MNP (Supplementary Figure 8S). When free in solution, Mms6 should be able to completely surround the growing MNP, having a greater effect on controlling size and shape. Therefore, Mms6 could mediate the crystallisation of larger MNPs when on a surface, as it is likely that the control it can exert on the formation of the MNP is altered by immobilisation to a substrate.

The types of material, size, shape and crystallinity of MNPs have a strong effect on their magnetic properties.[55] To minimise internal energy, bulk magnetic structures form randomly orientated regions of uniform magnetisation called domains, so that magnetostatic energy is minimised.[56] However, energy is also required to maintain the walls between domains.[56] As the particle size is reduced, the material forms a uniformly magnetised single domain MNP when it costs more energy to create a domain wall than to support the magnetostatic energy.[56] As the size of the MNP is reduced further, the superparamagnetic limit is reached, as thermal energy exceeds the magnetic anisotropy energy of the particle.[56] The upper limit for MNPs of spherical and cubic magnetite to behave superparamagnetically is approximately 25 nm, so magnetite MNPs bellow this size could not retain their magnetisation direction in the absence of an applied field.[57] Above ≈85 nm, MNPs of magnetite form multi-domain particles.[58] The controlled doping of cobalt into magnetite alters the magnetic properties. A preferred axis of magnetisation is introduced, increasing the coercivity. MNPs of cobalt ferrite are able to maintain a single domain in a decreased size range, between 5 nm[59] and 70 nm.[60] Although an exact literature value has yet to be published, if a linear relationship is assumed, it is expected that MNPs of 6% cobalt-doped magnetite will maintain a single domain above approximately 20 nm in diameter.[30]

To be used successfully within technologies, each MNP is required to be highly uniform, to ensure a consistent magnetic response. In this study, Mms6 is seen to exert control over the size of the particles formed on the patterned surfaces, biotemplating particles with a much tighter size distribution than those that formed in the bulk reactions. In particular, the number of small particles within the superparamagnetic size region is significantly reduced, making the magnetic behaviour of the Mms6 surface templated MNPs very uniform, and thus highly applicable for use in technologies.

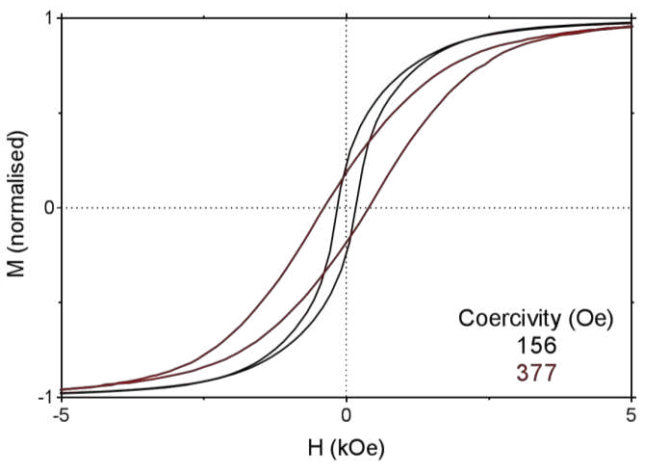

Figure 5: Magnetic hysteresis loops recorded using VSM at 295 K of MNPs biotemplated onto gold surfaces by Mms6, without (black) and with (red) the addition of 6% Co. These loops show an increase in coercivity for the cobalt-doped surface (377 Oe) when compared to the undoped surface (156 Oe).

We obtained magnetic hysteresis loops using vibrating sample magnetometry (VSM) at room temperature (295 K) for both $Fe_{surface}$ and $6\%Co_{surface}$ samples (Figure 5). The magnetisation of the loops has been normalised, as MNPs on the surfaces could not be accurately quantified. Figure 5 shows how the addition of 6% cobalt increases the coercivity of the MNPs that were biotemplated onto the surface ($Fe_{Surface}$: ≈156 Oe, $6\%Co_{Surface}$: ≈377 Oe). This highlights the adaptability of this approach, with the simple addition of cobalt to the POFHK reaction allowing the coercivity (magnetic hardness) of the MNPs to be fine-tuned between that of magnetite and cobalt ferrite.

The coercivity recorded for the $Fe_{Surface}$ MNPs is larger than what has been previously reported in the literature,[61] and this could be a cooperative effect resulting from the fact that the particles are bound to a surface. This is supported by the coercivity recorded with VSM of the Fe_{Bulk} MNPs (≈110Oe, Supplementary Figure 9S), which is within the range of published values.[61] Although the addition of 6% cobalt more than doubles the coercivity of the biotemplated MNPs, current recoding mediums used within magnetic data storage devices contain magnetic thin-films with coercivities in the kOe range.[10] While this study presents a significant step towards the development of biotemplated bit-patterned media, further development is required before biotemplated data storage becomes a reality.

The nanomagnetic properties of the MNP arrays, biotemplated by Mms6 onto the gold surfaces, were studied with magnetic force microscopy (MFM) (Figure 6). These MFM plots show that zones of attraction and repulsion (red and blue areas respectively in Figure 6) formed over both the $Fe_{Surface}$ and $6\%Co_{Surface}$ biotemplated MNPs. No magnetic information was recorded when MFM was performed with a non-magnetic tip, and these zones were found to be stable and unchanging when different scan directions were used (Supplementary Figure 10S and 11S). This shows that both the $Fe_{Surface}$ and $6\%Co_{Surface}$ MNPs are ferrimagnetic, maintaining their magnetic orientation at room temperature, and that the zones of attraction and repulsion are not altered by scanning the magnetised tip above the surfaces.

MFM measurements of $6\%Co_{Surface}$ samples also revealed that magnetic zones of attraction and repulsion extend over larger distances than the undoped $Fe_{Surface}$ samples. This can be seen more clearly when MFM measurements were performed on $6\%Co_{Surface}$ surfaces containing MNP line patterns with a larger line-width than the ≈1 μm lines displayed in Figure 6 (Supplementary Figure 3S). This may be an effect of the 6% cobalt doping, which increases the coercivity of the doped MNPs making the direction of magnetisation more difficult to perturb at room temperature. As a result the 6% cobalt-doped MNP could be able to form more stable interactions on the 2D surface. However, the microscale lines of MNPs that were biomineralised onto the gold surfaces by Mms6 make it difficult to probe the nanomagnetism of individual MNPs with MFM. For this to become possible the magnetic complexity would have to be reduced through the patterning of Mms6 on the nanoscale.

In this study, we patterned Mms6 on a scale approaching the limits of μCP (≈1 μm).[62] There now are now a large number of techniques available with the capability of patterning SAMs, such as the PEG used in this study, with sub-micrometre dimensions. As a result, the approach introduced in this study could easily be adapted to push the patterning of Mms6 into the nanoscale. The use of composite PDMS stamps, containing a stiff layer supported by a more flexible layer, has been shown to extend the patterning resolution of μCP to <100 nm.[62] Another approach is interferometric lithography (IL),[63] whereby a SAM surface is patterned using the interference of UV light, which leads to spatially defined photocatalytic degradation. This technique has the ability to form a fast and efficient route for the production of precise nanoscale SAM patterns, with the potential to form a more industrially scalable route for the patterning of biomolecules such as Mms6.

The bioinspired approach introduced in this study is highly adaptable, with the possibility to use other biomineralising proteins and peptides for the production of a wide range of different biotemplated nanomaterials on surfaces. These are no longer limited to naturally occurring proteins and peptides. Techniques such as biopanning have uncovered numerous novel biomolecules that can interact with many different materials.[64] The patterning and immobilisation of these biomolecules could open up new routes for the production of many different nanomaterials on surfaces, and lead to the development of a whole new range of biotemplated materials for a vast array of different technologies.

The method presented in this study forms a new methodology for the synthesis of biotemplated surfaces, which could be adapted with the aim of developing biotemplated bit-patterned media. One of the most promising approaches is the patterning of FePt or CoPt MNPs, which can be synthesised with nanoparticle diameters of a few nanometres, and still maintain their single magnetic domain.[65, 66 67] Yet there are many challenges to overcome before these MNPs can be successfully patterned onto a substrate to form a recording medium. The main challenge is synthesising the $L1_0$ phase for MNPs without annealing and aggregating the particles, something which has yet to be overcome.[68]

Biotemplating peptides have significantly reduced the temperatures and processing steps required to achieve the $L1_0$ platinum alloy phase.[69] In the future, it may be possible to optimise such biotemplating systems (by finding or designing new peptides, or optimising and doping mineralisation protocols) to avoid the need for annealing to achieve the $L1_0$ phase. It may also be possible to adapt the cys-Mms6 array synthesis introduced in this study to form thin-films and patterns of $L1_0$ platinum alloys onto surfaces (also see Galloway et al.[19]). Demonstrating that biotemplated magnetic materials are comparable, or even better than, synthetic

analogues, would lead to truly greener, cleaner, biotemplated data storage. The bioinspired approach introduced in this paper provides a versatile platform that could be exploited and adapted with alternative patterning techniques, biomolecules and mineralisation protocols to develop such systems, and bring biotemplated bit-patterned media closer to reality.

Conclusions

The soft lithographic technique of μCP was used to pattern a cys-mutated version of the biomineralisation protein Mms6, which binds directly to gold via an N-terminal cysteine. The immobilised protein templated the formation of highly uniform MNPs on micropatterned lines under mild reaction conditions. Furthermore, these MNPs are ferrimagnetic, and able to maintain their direction of magnetisation at room temperature. The controlled doping of cobalt into the system produced magnetically harder MNPs, allowing the magnetic properties of these biotemplated MNPs to be fine-tuned. This simple and bioinspired approach is highly adaptable, with the possibility to use other patterning techniques, biomineralising proteins and peptides for the production of precise patterns of technologically relevant nanomaterials, and makes significant strides towards the production of environmentally friendly, biotemplated MNP arrays for nanotechnologies such as ultra-high-density data-storage.

Acknowledgements

The authors would like to thank the LENNF facility at the University of Leeds and Stuart Micklethwaite for assistance with SEM and EDX, and Stephen Baldwin for the pTTQ18 based parent vector. We would also like to thank Rebecca Savage and Jamie Hobbs for their help with obtaining MFM images, Nik Reeves-McLaren for support with XRD, Neil Bramall for the collection of ICP-ES data at the University of Sheffield. We also thank Paul Steadman, Alexey Dobrynin and Peter Bencok at the Diamond light source for all their efforts during the experiments at Diamond, and Neil Telling for advice with analysing this data.

We thank the BBSRC (BB/H005412/2) for funding this work and the EPSRC for funding Scott Bird (CDT studentship (EP/J500458/1)) and Johanna Galloway (Post-Doctoral Prize Fellowship (EP/K503071/1)).

Notes and references

[a] University of Sheffield, Department of Chemistry, Dainton Building, Sheffield, S3 7HF, UK.

[b] University of Leeds, Department of Physics & Astronomy, E C Stoner Building, Leeds, LS2 9JT, UK.

[c] The program used to render the MFM images in 3D is available here: https://github.com/jonbramble/MFMPlot

1. L. H. Reddy, J. L. Arias, J. Nicolas and P. Couvreur, Chemical reviews, 2012, 112, 5818-5878.
2. S. Laurent, D. Forge, M. Port, A. Roch, C. Robic, L. Vander Elst and R. N. Muller, Chemical reviews, 2008, 108, 2064-2110.
3. M. Faraji, Y. Yamini and M. Rezaee, Journal of the Iranian Chemical Society, 2010, 7, 1-37.
4. S. C. Tsang, V. Caps, I. Paraskevas, D. Chadwick and D. Thompsett, Angewandte Chemie, 2004, 116, 5763-5767.
5. D. Zhang, S. Wei, C. Kaila, X. Su, J. Wu, A. B. Karki, D. P. Young and Z. Guo, Nanoscale, 2010, 2, 917-919.
6. U. Jeong, X. Teng, Y. Wang, H. Yang and Y. Xia, Adv. Mater., 2007, 19, 33-60.
7. S. Mornet, S. Vasseur, F. Grasset, P. Veverka, G. Goglio, A. Demourgues, J. Portier, E. Pollert and E. Duguet, Progress in Solid State Chemistry, 2006, 34, 237-247.
8. A. K. Gupta and M. Gupta, Biomaterials, 2005, 26, 3995-4021.
9. B. Terris and T. Thomson, Journal of physics D: Applied physics, 2005, 38, R199.
10. S. Piramanayagam and T. C. Chong, Developments in data storage: materials perspective, John Wiley & Sons, 2011.
11. S. H. Charap, P.-L. Lu and Y. He, Magnetics, IEEE Transactions on, 1997, 33, 978-983.
12. B. Terris, T. Thomson and G. Hu, Microsystem technologies, 2007, 13, 189-196.
13. R. A. Metzler, I. W. Kim, K. Delak, J. S. Evans, D. Zhou, E. Beniash, F. Wilt, M. Abrecht, J.-W. Chiou and J. Guo, Langmuir, 2008, 24, 2680-2687.
14. J. M. Galloway and S. S. Staniland, Journal of Materials Chemistry, 2012, 22, 12423-12434.
15. B. Wang, K. Chen, S. Jiang, F. Reincke, W. Tong, D. Wang and C. Gao, Biomacromolecules, 2006, 7, 1203-1209.
16. R. R. Naik, S. J. Stringer, G. Agarwal, S. E. Jones and M. O. Stone, Nature materials, 2002, 1, 169-172.
17. B. D. Reiss, C. Mao, D. J. Solis, K. S. Ryan, T. Thomson and A. M. Belcher, Nano letters, 2004, 4, 1127-1132.
18. M. T. Klem, D. Willits, D. J. Solis, A. M. Belcher, M. Young and T. Douglas, Advanced Functional Materials, 2005, 15, 1489-1494.
19. J. M. Galloway, S. M. Bird, J. P. Bramble, K. Critchley and S. S. Staniland, MRS Proceedings, 2013, 1569, 231-237.
20. E. Mayes, A. Bewick, D. Gleeson, J. Hoinville, R. Jones, O. Kasyutich, A. Nartowski, B. Warne, J. Wiggins and K. Wong, Magnetics, IEEE Transactions on, 2003, 39, 624-627.
21. I. Yamashita, H. Kirimura, M. Okuda, K. Nishio, K. I. Sano, K. Shiba, T. Hayashi, M. Hara and Y. Mishima, Small, 2006, 2, 1148-1152.
22. M. Uchida, M. T. Klem, M. Allen, P. Suci, M. Flenniken, E. Gillitzer, Z. Varpness, L. O. Liepold, M. Young and T. Douglas, Adv. Mater., 2007, 19, 1025-1042.
23. J. Hoinville, A. Bewick, D. Gleeson, R. Jones, O. Kasyutich, E. Mayes, A. Nartowski, B. Warne, J. Wiggins and K. Wong, Journal of applied physics, 2003, 93, 7187-7189.
24. S. Bellini, Chinese Journal of Oceanology and Limnology, 2009, 27, 3-5.
25. S. Bellini, Chinese Journal of Oceanology and Limnology, 2009, 27, 6-12.
26. R. Blakemore, Science, 1975, 190, 377-379.
27. A. Arakaki, J. Webb and T. Matsunaga, Journal of Biological Chemistry, 2003, 278, 8745-8750.
28. J. M. Galloway, A. Arakaki, F. Masuda, T. Tanaka, T. Matsunaga and S. S. Staniland, J. Mater. Chem., 2011, 21, 15244-15254.

29. Y. Amemiya, A. Arakaki, S. S. Staniland, T. Tanaka and T. Matsunaga, Biomaterials, 2007, 28, 5381-5389.
30. J. M. Galloway, A. Arakaki, F. Masuda, T. Tanaka, T. Matsunaga and S. S. Staniland, Journal of Materials Chemistry, 2011, 21, 15244-15254.
31. L. Wang, T. Prozorov, P. E. Palo, X. Liu, D. Vaknin, R. Prozorov, S. Mallapragada and M. Nilsen-Hamilton, Biomacromolecules, 2011, 13, 98-105.
32. A. Arakaki, F. Masuda and T. Matsunaga, MRS Proceedings, 2009, 1187, KK03-08.
33. J. M. Galloway, J. P. Bramble, A. E. Rawlings, G. Burnell, S. D. Evans and S. S. Staniland, Journal of Nano Research, 2012, 17, 127-146.
34. J. M. Galloway, J. P. Bramble, A. E. Rawlings, G. Burnell, S. D. Evans and S. S. Staniland, Small, 2012, 8, 204-208.
35. R. V. Duevel and R. M. Corn, Analytical Chemistry, 1992, 64, 337-342.
36. F. W. Studier, Protein expression and purification, 2005, 41, 207-234.
37. K. L. Prime and G. M. Whitesides, Journal of the American Chemical Society, 1993, 115, 10714-10721.
38. A. Regazzoni, G. Urrutia, M. Blesa and A. Maroto, Journal of Inorganic and Nuclear Chemistry, 1981, 43, 1489-1493.
39. Ł. Krzemiński, S. Cronin, L. Ndamba, G. W. Canters, T. J. Aartsma, S. D. Evans and L. J. Jeuken, The Journal of Physical Chemistry B, 2011, 115, 12607-12614.
40. M. V. Voinova, M. Rodahl, M. Jonson and B. Kasemo, Physica Scripta, 1999, 59, 391.
41. C. Zhou, J.-M. Friedt, A. Angelova, K.-H. Choi, W. Laureyn, F. Frederix, L. A. Francis, A. Campitelli, Y. Engelborghs and G. Borghs, Langmuir, 2004, 20, 5870-5878.
42. C. A. Schneider, W. S. Rasband and K. W. Eliceiri, Nat Meth, 2012, 9, 671-675.
43. G. Prism, Graphpad: La Jolla, CA, USA, 2013.
44. A. Patterson, Physical review, 1939, 56, 978.
45. I. Horcas, R. Fernandez, J. Gomez-Rodriguez, J. Colchero, J. Gómez-Herrero and A. Baro, Review of Scientific Instruments, 2007, 78, 013705.
46. D. Xu and Y. Zhang, Proteins, 2012, 80, 1715-1735.
47. S. McNicholas, E. Potterton, K. Wilson and M. Noble, Acta Crystallographica Section D: Biological Crystallography, 2011, 67, 386-394.
48. G. Sauerbrey, Physics, 1959, 155, 206-222.
49. M. Rodahl, F. Höök, C. Fredriksson, C. A. Keller, A. Krozer, P. Brzezinski, M. Voinova and B. Kasemo, Faraday discussions, 1997, 107, 229-246.
50. A. Kihal, B. Bouzabata, G. Fillion and D. Fruchart, Physics Procedia, 2009, 2, 665-671.
51. M. Sorescu, A. Grabias, D. Tarabasanu-Mihaila and L. Diamandescu, Journal of Materials Synthesis and Processing, 2001, 9, 119-123.
52. T. Prozorov, P. Palo, L. Wang, M. Nilsen-Hamilton, D. Jones, D. Orr, S. K. Mallapragada, B. Narasimhan, P. C. Canfield and R. Prozorov, ACS nano, 2007, 1, 228-233.
53. N. Telling, V. Coker, R. Cutting, G. van der Laan, C. Pearce, R. Pattrick, E. Arenholz and J. Lloyd, Applied Physics Letters, 2009, 95, 163701-163701-163703.
54. R. C. Rodrigues, C. Ortiz, Á. Berenguer-Murcia, R. Torres and R. Fernández-Lafuente, Chemical Society Reviews, 2013, 42, 6290-6307.
55. A. H. Lu, E. e. L. Salabas and F. Schüth, Angewandte Chemie International Edition, 2007, 46, 1222-1244.
56. S. Blundell and D. Thouless, American Journal of Physics, 2003, 71, 94-95.
57. D. Dunlop, Journal of Geophysical Research, 1973, 78, 1780-1793.
58. B. M. Moskowitz and S. K. Banerjee, Magnetics, IEEE Transactions on, 1979, 15, 1241-1246.
59. N. Moumen, P. Bonville and M. Pileni, The Journal of Physical Chemistry, 1996, 100, 14410-14416.
60. A. Berkowitz, W. Schuele and P. Flanders, Journal of Applied Physics, 1968, 39, 1261-1263.
61. M. Ma, Y. Wu, J. Zhou, Y. Sun, Y. Zhang and N. Gu, Journal of Magnetism and Magnetic Materials, 2004, 268, 33-39.
62. T. W. Odom, J. C. Love, D. B. Wolfe, K. E. Paul and G. M. Whitesides, Langmuir, 2002, 18, 5314-5320.
63. G. Tizazu, O. El-Zubir, S. R. Brueck, D. G. Lidzey, G. J. Leggett and G. P. Lopez, Nanoscale, 2011, 3, 2511-2516.
64. C. Tamerler, S. Dinçer, D. Heidel, N. Karaguler and M. Sarikaya, 2003.
65. S. Sun, C. B. Murray, D. Weller, L. Folks and A. Moser, Science, 2000, 287, 1989-1992.
66. T. O. Ely, C. Pan, C. Amiens, B. Chaudret, F. Dassenoy, P. Lecante, M.-J. Casanove, A. Mosset, M. Respaud and J.-M. Broto, The Journal of Physical Chemistry B, 2000, 104, 695-702.
67. D. Weller, A. Moser, L. Folks, M. E. Best, W. Lee, M. F. Toney, M. Schwickert, J.-U. Thiele and M. F. Doerner, Magnetics, IEEE Transactions on, 2000, 36, 10-15.
68. T. Thomson, M. Toney, S. Raoux, S. Lee, S. Sun, C. Murray and B. Terris, Journal of applied physics, 2004, 96, 1197-1201.
69. C. Mao, D. J. Solis, B. D. Reiss, S. T. Kottmann, R. Y. Sweeney, A. Hayhurst, G. Georgiou, B. Iverson and A. M. Belcher, Science, 2004, 303, 213-217.

ARTICLE

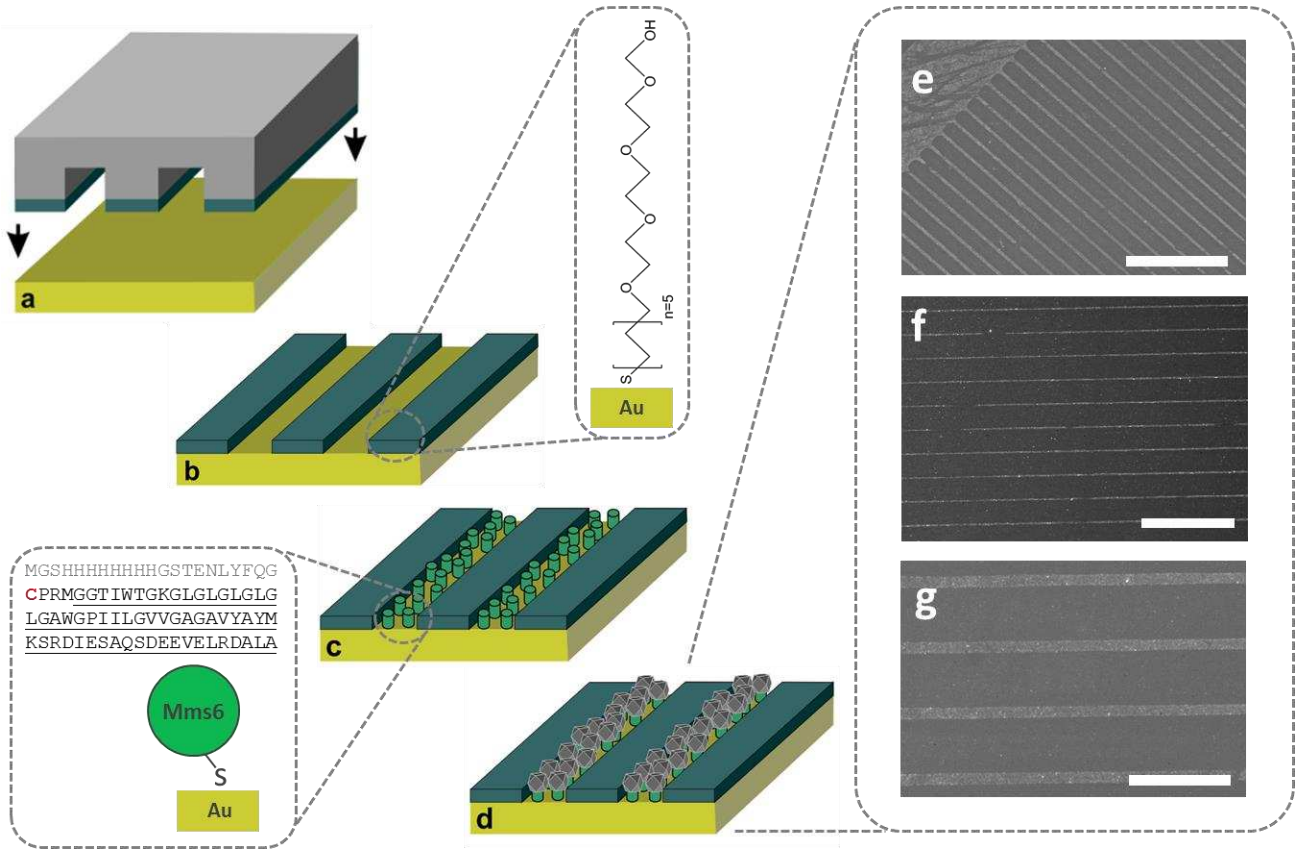

Figure 2: Schematic representing the stages involved in biotemplating the MNP arrays (a-d) and SEM images (e-g) of the biotemplated arrays formed (scale bars e: 100 µm, f: 25 µm and g: 25 µm). a) A flexible polymer stamp is inked with a PEG thiol (dark green) and placed in conformal contact with a gold surface. b) After 4 minutes the stamp is removed, allowing time for an anti-biofouling PEG SAM to form where the stamp met the surface (the structure of which is shown). c) The cysteine-tagged Mms6 protein (light green cylinders) binds to the bare gold areas (the amino acid sequence of the Mms6 protein is also shown with the purification tag greyed out, the N-terminal cysteine in red and the Mms6 mature sequence underlined). d) When immersed in a POFHK reaction designed to form magnetite or 6% cobalt-doped magnetite MNPs (dark crystals) form on the areas patterned with Mms6.

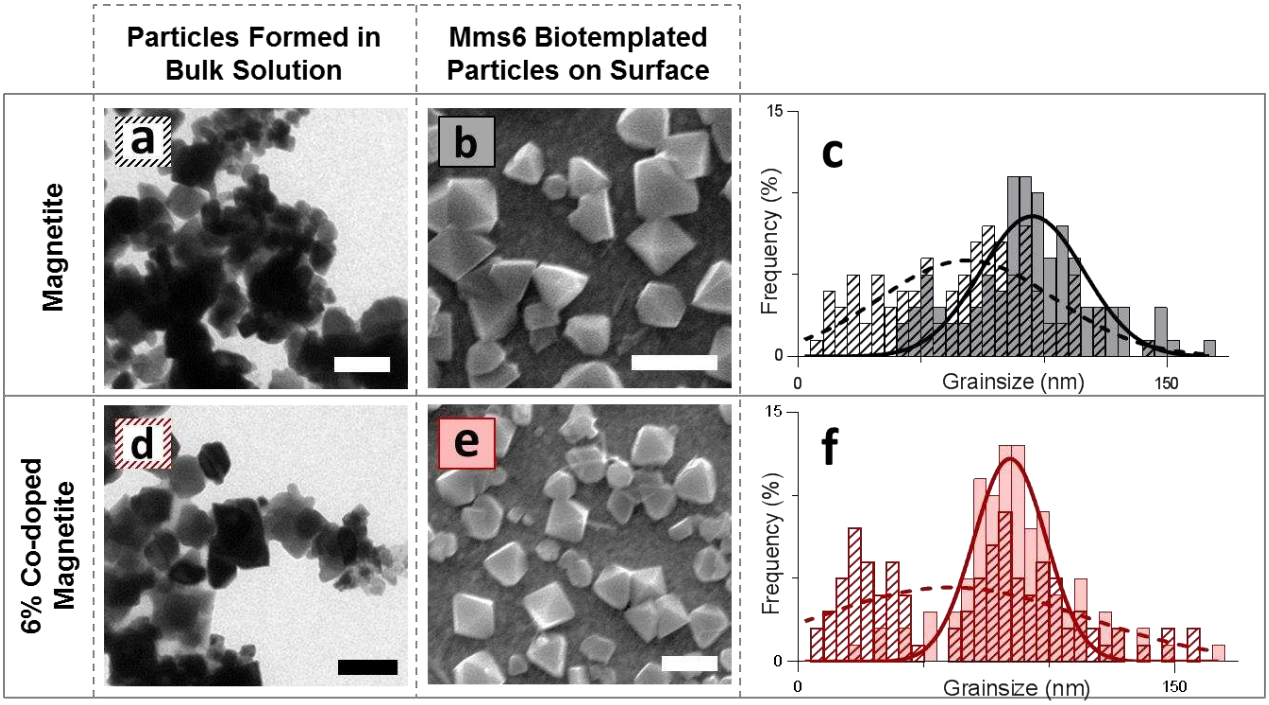

Figure 4: TEM (a.d) images of MNPs that formed in solution during a POFHK reaction and SEM (b,e) images of MNPs biotemplated onto gold by immobilised Mms6 (scale bars 100 nm). c,f) Grain size analysis based on ≈100 MNPs per sample. The longest axis of the MNP projections in TEM and SEM images was measured using ImageJ, [45] and results were plotted and fitted with a Gaussian distribution in GraphPad Prism software.[46]. a,b,c) MNPs formed during a POFHK reaction designed to produce magnetite. d,e,f) MNPs formed during a POFHK reaction with the addition of 6% cobalt. The MNPs biotemplated onto the surface appear to be highly uniform, and were found to have a larger mean size and narrower size distribution ($Fe_{Surface}$: ≈90±15 nm and 6%$Co_{Surface}$: ≈84±14 nm) than those from the bulk solution (Fe_{Bulk}: ≈69±36 nm and 6%Co_{Bulk}: ≈61±53 nm).

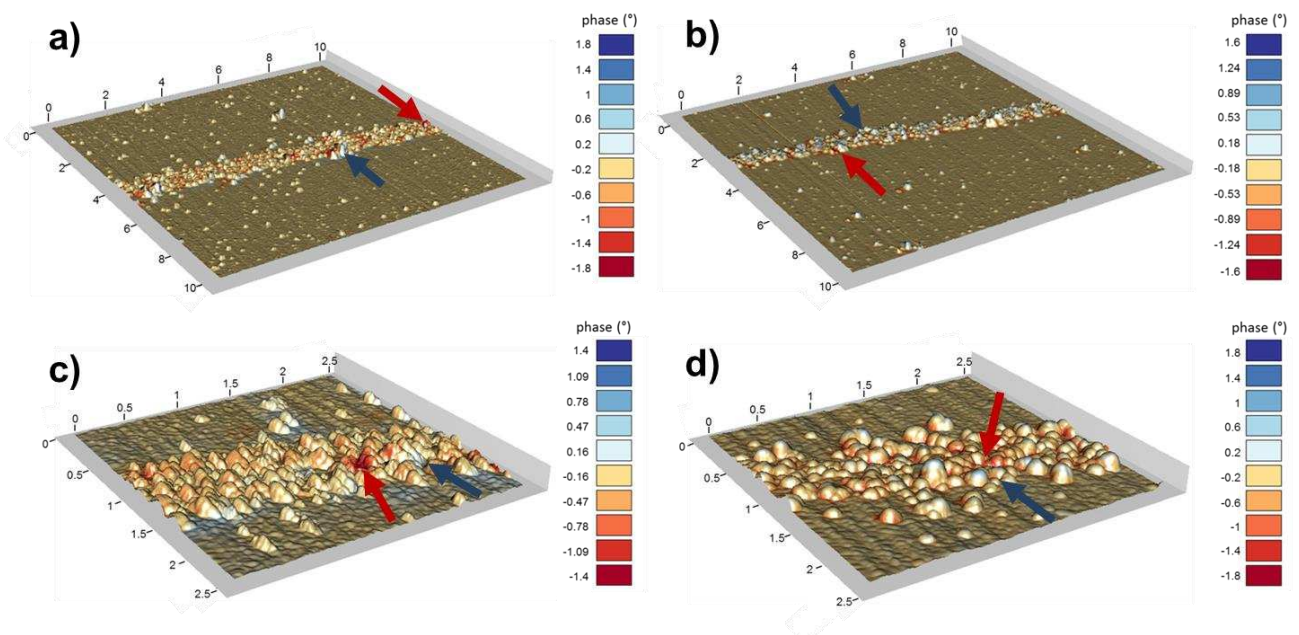

Figure 6: Composite images of topography obtained with tapping mode AFM and MFM phase sift at a lift height of 50 nm of magnetite (a and c) and 6% cobalt-doped magnetite (b and d) MNPs biotemplated by Mms6 onto gold (x and y scales are in µm). Zones of attraction and repulsion (red and blue areas, some example areas are highlighted by red and blue arrows) were found to form, suggesting that the biotemplated MNPs are ferrimagnetic and able to maintain their magnetisation at room temperature.